Arabian Journal of Chemistry (2020) 13, 3639–3652

King Saud University

Arabian Journal of Chemistry

www.ksu.edu.sa
www.sciencedirect.com

ORIGINAL ARTICLE

An in-situ synthesis of novel V_2O_5/G-C_3N_4/PVA nanocomposite for enhanced electrocatalytic activity toward sensitive and selective sensing of folic acid in natural samples

Annamalai Karthika [a], **Ayyadurai Suganthi** [a,*], **Muthuramalingam Rajarajan** [b,*]

[a] *PG & Research Department of Chemistry, Thiagarajar College, Madurai 625009, Tamil Nadu, India*
[b] *Madurai Kamaraj University, Madurai 625 02, Tamil Nadu, India*

Received 2 November 2019; accepted 23 December 2019
Available online 27 December 2019

KEYWORDS

Electrochemical Sensor;
FA detection;
In-situ oxidative polymerization;
Amperometric method

Abstract This paper describes a highly sensitive and selective electrochemical sensing of folic acid (FA) using vanadium pentoxide decorated graphene carbon nitride covalently grafted polyvinyl alcohol modified GC electrode (V_2O_5/G-C_3N_4/PVA/GCE). The V_2O_5/G-C_3N_4/PVA nanocomposite was synthesized by an in-situ oxidative polymerization method and characterized by various techniques such as UV–visible, Raman, FE-SEM, XRD, FT-IR, EDX, HR-TEM, SAED, and electrochemical methods. The V_2O_5/G-C_3N_4/PVA nanocomposite modified GCE showed superior electrocatalytic activity towards the FA detection. The superior electrochemical activity of the catalyst is owing to good conductivity, high surface area and enhanced electron transfer efficiency of the nanocomposite. The amperometric (i-t) studies revealed that the V_2O_5/G-C_3N_4/PVA nanocomposite modified GCE performed well by attaining a linear response of FA from 0.01 to 60 μM with a lower detection limit 0.00174 μM and the sensitivity of 19.02 μA μM^{-1} cm^{-2}. Meanwhile, the V_2O_5/G-C_3N_4/PVA nanocomposite modified GCE exhibited good selectivity, rapid and stable response towards FA. The proposed method has been successfully applied for the selective determination of FA in various real samples such as apple juice, green tea and tap water with samples with good recoveries.

* Corresponding authors.
E-mail addresses: suganthitcarts@gmail.com (A. Suganthi), rajarajanchem1962@gmail.com (M. Rajarajan).
Peer review under responsibility of King Saud University.

Production and hosting by Elsevier

1. Introduction

Folic acid ((FA) $C_{19}H_{19}N_7O_6$) Scheme 1) is also called as Folate or folacin (anionic formation) and vitamin M in the form of vitamin B_9 is water-soluble. Folacin is also established in marmite or vegemite, with containing (1001 g) an average serving amount 5 g. It is also prepared by bacteria. Severalsig-

https://doi.org/10.1016/j.arabjc.2019.12.009
1878-5352

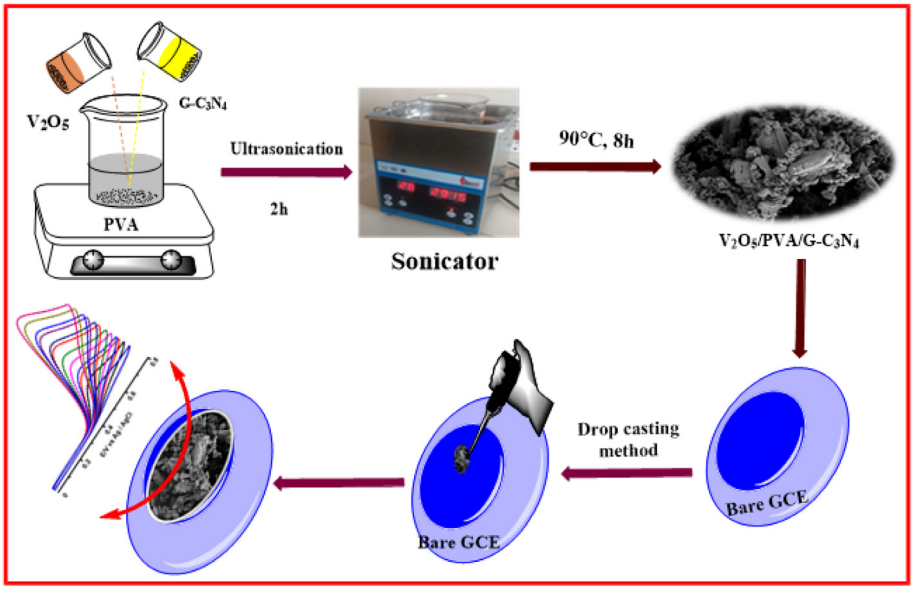

Scheme 1 Stepwise fabrication of V_2O_5/PVA/G-C_3N_4/GCE for FA detection.

nificant nutrients provide as building blocks of a well human pregnancy (Safaei et al., 2018; Lavanya et al., 2016;Ensafi and Maleh, 2010; Taherkhani et al., 2012). FAanindividual nutrient of enormoussubstance, especially for women'sdevelopment for pregnancy. Tolerable folate ingestion during the preconception time helps save from harm against several of habitual malformations. The most notable delivery defects that transpire from folate deficiency are neural tube defects, which consequence in malformations of the backbone (spina bifida), skull, and brain (anencephaly) (He et al., 2016). Women planning for pregnancy are advised to eat food fortified with FA or to take supplements in accumulation to ingestion folate-rich foods to decrease the hazard of severalgrave birth defects. Captivating 400 lg of artificialFAday by day from fortified foods and/or supplements has been suggested. The recommended dietary allowance (RDA) for folate equivalents for a pregnant lady is 600–800 μg, twice the normal RDA of 400 μg for women who were not pregnant (Zheng et al., 2017). Current investigate has shown that it is also vital for a man who isscheduling on fathering kids, reducing birth defects risks (Maleh et al., 2016; Araú jo et al., 2011). Generally, the concentration dosage level was increased and decreased and continuous usage of FA causes several critical issues such as gigantocytic anemia, several psychological disorders, alzheimer's disease, cardiovascular disease, stroke, heart attack, and cancer. Up to now, various analytical techniques such as HPLC-mass spectrometry (Zheng et al., 2015), Fluorimetric (Lapa et al., 1997), high-performance liquid chromatography (Young et al., 2011), thermo-gravimetry (Vora et al., 2002) chemiluminescence (Chen et al., 2019) spectrophotometry (Shishehbore et al., 2011) have been residential and utilized for the precise level detection of FA with tremendous sensitivity. Still, the aforementioned techniques are elevated cost, required specialist monitoring, complicated routine analysis, time-consuming, need anenormousquantity of reagents, highly skillful technician to control and tedious extraction progression (Fayemi et al., 2018). In its place of these, the electrochemical methods by using nanomaterials modified on the surface electrode are measured as progressiveequipment, because they offer several advantages than that of other techniques such as price valuable, portability, easy to use, precise, responsive, rapid answer, and selective FA detection(Naqvi et al., 2019;Keyvanfard et al., 2012; Mirmoghtadaie et al., 2013a, 2013b). Though, the straight oxidation of FA on the bare electrode shows pitiable response due to their transfer electron process and over oxidation potential peak. Therefore, lots of efforts have been made to expand a novel material for the improved and sensitive electrochemical study towards FA detection. Currently nanocomposite could be easily made by sono-chemical approaches. Inside a short period of time the nanoparticles could be easily formed by this method. The shaped sonication method is made by the formation of growth and collapses of liquid. Surrounded by a short period time the bubbles with concentrated energy are unconfined with a cooling and heating rate ($> 1010\ Ks^{-1}$). In addition, uniform bring together in this method provides good quality distribution and dispersion properties.

Vanadium pentoxides (V_2O_5) have newly established considerable attention for a selection of applications due to their unique physicochemical properties (Zhu et al., 2013). They have a variety of hopeful applications including catalysis, photocatalysis, lithium-ion batteries, hydrogen storage material, corrosion prevention, gas sensors, dye- solar cells sensitized, ultraviolet absorbents, conducting electrodes and so forth (Xu et al., 2013; Li et al., 2017a, 2017b). Accidently, their sensible applications are restricted by pitiable electron transfer efficiency, sensitivity, constancy, electrocatalytic motion, and durability. To keep away from these problems, V_2O_5 joint with the other carbon-based materials as behind backgrounds which carbon nanotubes, quantum dot, polydopamine, corporate graphene, graphitic carbon nitride mesoporous carbon, and conducting polymers because of their exclusivemechanical, electronic, physical, thermal, and chemical properties (Liu et al., 2019a, 2019b; Liu et al., 2018; Majumdar et al., 2019). Since most important leading synthetic polymer, polyvinyl alcohol assure for profitable applications, for the reason that,

it's emulsifying, adhesives, chemical resistance, hydrophilicity, and brilliant film-forming potential (Sathiya et al., 2011; Long et al., 2017). The eco-friendly nature of semi-crystalline polymer of PVA is due to its properties such as biodegradable as well as easily soluble in water. In most of the existing developments, V_2O_5 is hybridized with functional carbon-based materials (G-C_3N_4), to fabricate a smart material that exhibits large particular surface area, mobility, exclusive electrochemical properties and elevated charge capacity carrier (Shash, 2013). These nanocomposites too have their fashionable disadvantages and advantages. To develop the complete compensation of material nanocomposites, there are a small number of investigations by our set on the ternary nanocomposites in comparison withtheir variety ofpossible applications (Pravakar et al., 2019). A combination of exclusive properties of creature nanostructured material counterparts made by asynergistic effect, which enhances electrochemical excellent selectivity, renewability and sensitivity. Although this nanoparticle has stable at elevated temperature, pressure and having good active surface area. Hitherto, there is no study reported to scrutinize the instantaneousinvention of G-C_3N_4 grafting with PVA and decoration of V_2O_5 nanocomposite for electrochemical sensing.

In this present work, we have demonstrated a novelV_2O_5 decorated on G-C_3N_4 covalently grafted to PVA via in situ oxidative polymerization process, and a utilized as a modified electrode material for the FA detection. The prepared V_2O_5/G-C_3N_4/PVA nanocomposite was characterized by a variety of characterization in the physicochemical process. Fascinatingly, the V_2O_5/G-C_3N_4/PVA nanocomposite modified GCE exhibited an exceptional electrocatalytic activity and significant electroanalytical performance towards FA sense, when compared to V_2O_5/GCE, V_2O_5/PVA/GCE, V_2O_5/G-C_3N_4/GCE and unmodified GCE. We also demonstrated the sensible applicability of real sample analysis in folate tablet and human (spiked) blood serum, urine, orange juice, tomato juice, beetroot, papaya juice, broccoli samples based on V_2O_5/G-C_3N_4/PVA modified GCE and obtained acceptable recoveries.

2. Experimental section

2.1. Reagents and instruments

Vanadium pentoxide, PVA, Urea, Folic acid (FA), Dopamine (DA), Cysteine (Cys), Ascorbic acid (AA), Glucose (Glu), Norepinephrine (Nep), Epinephrine (Ep), Sucrose (Suc), and Uric acid obtainedcompany from sigma Aldrich. Phosphate buffer usedlike a supporting electrolyte, which is prepared by mixing of Na_2HPO_4 and NaH_2PO_4, the pH was used to by adding orthophosphoric acid and sodium hydroxide. The entire required store solutions were prepared by using distilled water was used for the entire electrochemical studies. All the electrochemical experiment studies were measured in the deoxygenated (N_2 atmosphere) electrolyte solution at room temperature.

FT-IR spectrum (Functional group) was recorded by using the JASCO-6600 instrument. The crystallographic structure was investigated by XRD using JDX-JEOL with Cu Ka (8030) radiation at a40 kV operating voltage was used. Raman spectroscopy was recorded by using WI-Tech CRM- 200. The morphology sizes and shape were carried out by FE-SEM modelCarl Zeiss, Germany (Supra 35-VP) and 15 kV operated and HR-TEM images were carried out by G2-TECNAI microscope. UV–Vis spectra were carried out by Jasco (V-560) model. The three-electrode system was used for the electrochemical experiments in the cell model-660E (Austin-TX, USA). All experiments were carried out at room temperature.

2.2. Synthesis of V_2O_5/PVAnanocomposite

0.5 g of PVA and 5 g of V_2O_5 (1:10 ratio) was dissolved in 50 ml DD water followed by ultrasonicated (300 W) for 2 h. The obtained precipitate solution was stirred 30 min for magnetic stirrer and dropwise added 0.1 M NaOH (2 N) solution. Hence, the mixture solution was stirred and heated with 60 °C for 30 min. The precipitate solution was washed with ethanol and water and dried in the oven at 80 °C for 10 h. Then the nanocomposite was kept in muffle furnace and calcinated at 300 °C for 2 h, V_2O_5/PVAnanocomposite was obtained.

2.3. Synthesis of V_2O_5/PVA/G-C_3N_4 nanocomposite

In a typical procedure, G-C_3N_4 was synthesized by the polycondensation process (Amanulla et al., 2018) 0.0.1 M G-C_3N_4 (0.59 mg in 30 ml) and 0.5 M (5 g in 30 ml) V_2O_5/PVA (1:10 ratio) were mixed in a 100 ml beaker and allowed to ultrasonication bath (300 W) for 2 h. Then the resultant pale orange product was gently collected by centrifugation and washed thoroughly with ethanol and water several times and dried at 90 °C for 8 h. The general synthesis method and the applications of V_2O_5/PVA/G-C_3N_4 nanocomposite are illustrated in Scheme 1.

2.4. Fabrication of V_2O_5/PVA/G-C_3N_4 modified glassycarbon electrode

Before the surface modification, the surface of GCE was well polished with 0.3 μm alumina powder, smoothly washed with ethanol, acetone, and water to take away the adsorbed alumina and dried at room temperature. The V_2O_5/PVA/G-C_3N_4 was re-dispersed in DD water at a concentration of 5 mg/mL with the assistance of ultrasonication for 15 min; consequential in a uniform white suspension was presented. Finally, exceeding 7 μL of V_2O_5/PVA/G-C_3N_4 suspension was drop cast on the surface of GCE and it was permitted to dry in the normal temperature. The obtained electrode was noted as V_2O_5/PVA/G-C_3N_4 and it was used for electrochemical measurements.

3. Result and discussion

3.1. Characterization

The optical property of the prepared V_2O_5, V_2O_5/PVA, V_2O_5/G-C_3N_4, V_2O_5/PVA/G-C_3N_4 nanocomposite was characterized via UV–Vis spectroscopy. Fig. 1Aa and bshows two absorption peak has appeared in 204–258 nm of V_2O_5. When PVA dopedwithV_2O_5, a shoulder band is observed at the same wavelength indicated and displayed in Fig. 1Ab. As seen in Fig. 1Ac and d the (V_2O_5/G-C_3N_4, V_2O_5/PVA/G-C_3N_4) broadband is observed at 205 nm-260 nm and 204 nm to 262 nm

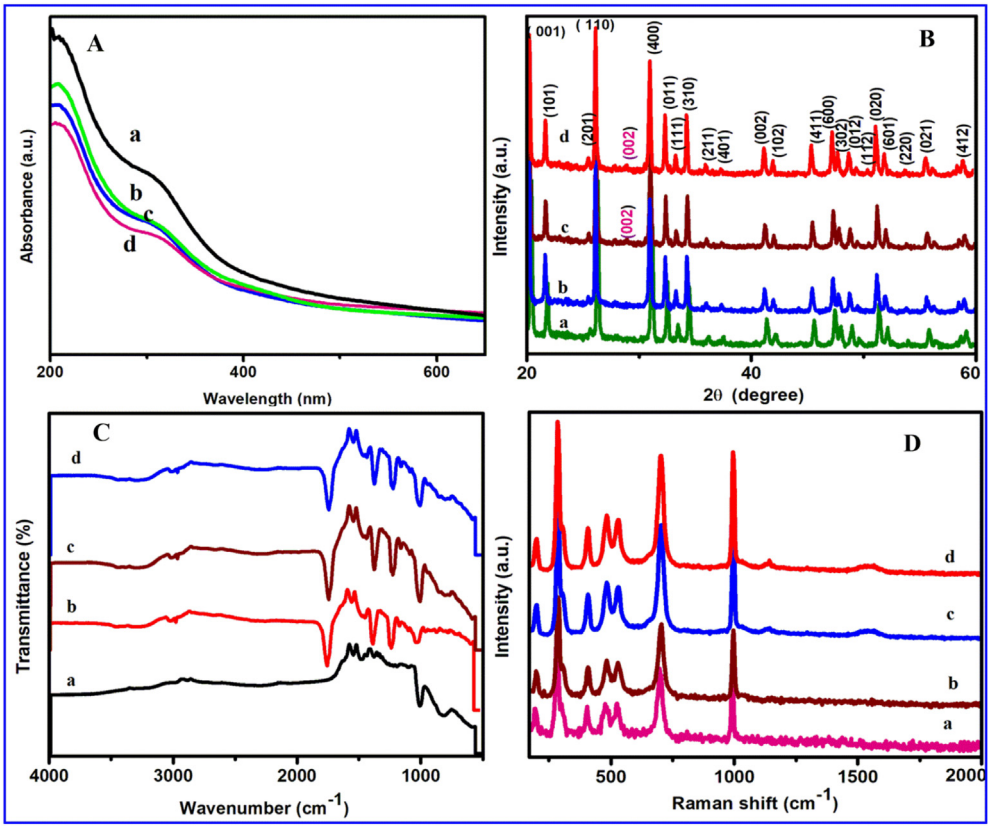

Fig. 1 (A) UV–visible spectrum of (a) V_2O_5 (block line), (b) V_2O_5/PVA (green line), (c) V_2O_5/G-C_3N_4 (blue line), and V_2O_5/PVA/G-C_3N_4 (rose line) nanocomposite, (B) XRD pattern of (a) V_2O_5 (green), (b) V_2O_5/PVA (blue), (c) V_2O_5/G-C_3N_4 (merun), and V_2O_5/PVA/G-C_3N_4 nanocomposite (red), (C) FT-IR spectrum of (a) V_2O_5 (ink blue), (b) V_2O_5/PVA (red), (c) V_2O_5/G-C_3N_4 (merun), and V_2O_5/PVA/G-C_3N_4 nanocomposite (blue), (D) Raman spectra of (a) V_2O_5 (rose), (b) V_2O_5/PVA (merun), (c) V_2O_5/G-C_3N_4 (blue), and V_2O_5/PVA/G-C_3N_4 nanocomposite (red).

respectively. These results revealed that the PVA and V_2O_5 embedded on g-C_3N_4 surface which may be via charge transfer interaction, physisorption, and electrostatic binding. Fig. 1B (a–d) shows the crystallographic nature of the synthesized material was investigated by the X-ray diffraction method. Fig. 1Ba shows, the pure V_2O_5 phase (JCPDF 41-1426), corresponds well to thestructure of orthorhombic, with lattice parameters such as a = 11.516 Å, b = 3.566 Å and c = 4.373 Å have appeared respectively. Also PVA supported V_2O_5 nanosheet, while increased with the crystallinity of composite peak was shifted towards 2θ value is higher as illustrated in Fig. 1Bb. As presented in Fig. 1Bc, One new peak can be observed for pure g-C_3N_4 as displayed in Fig. 1Bc at 2 θ = 28.3°, which is ascribed to amorphous G-C_3N_4. Moreover, the diffraction peaks of G-C_3N_4 and V_2O_5/PVA appear in the curves of V_2O_5/PVA/G-C_3N_4 composites as exposed in Fig. 1Bd, signifying that the three components peaks are successfully hybridized (Darkwah and Oswald, 2019, Dou et al., 2019).

The chemical composition and bond analysis were examined for the as-prepared V_2O_5, V_2O_5/PVA; V_2O_5/G-C_3N_4; V_2O_5/PVA/G-C_3N_4 nanocomposite was investigated by FT-IR spectrum. The FT-IR spectrum of V_2O_5 (Fig. 1Ca) exhibits indicates the presence of the (V═O) symmetrical peaks appeared at 998 cm^{-1} respectively. The peaks at 799 and 533 $cm^{-1}$are assigned to the V—O stretching and V—O—V bending vibration, which may well be ascribed to stretching vibration of the O—H bond of water molecules. As well as another peak at 1600 cm^{-1} assigned to sharp vibration of water molecules. Besides PVA, the broad absorption range at 3445 cm^{-1} was attributed in the H—O—H band observed in water molecules. The spectrum of PVA describes the peaks at 2,854 cm^{-1} for the incidence of symmetric and asymmetric —CH_2 stretching vibration respectively. Symmetric stretching of carboxylate anion —COO represents an absorption band at 1,641 cm^{-1}. Fig. 1C c and d(V_2O_5/G-C_3N_4, V_2O_5/PVA/G-C_3N_4), from the peak 3305 to 3000 cm^{-1} is attributed to the stretching vibration modes of N-H bonds resulting from the incomplete condensation of amino groups. The ascribed the absorption peaks appeared at 889 and 806 $cm^{-1}$are attributed to the usualvibration units mode of tri-s-triazine and the twist mode of N-H bonds, respectively. A sequence of peak was observed 1700–1200 cm^{-1} in the range was indicates to the characteristic stretching modes of CN hetero-cycles.

Raman spectra of V_2O_5, V_2O_5/PVA, V_2O_5/G-C_3N_4, and V_2O_5/G-C_3N_4/PVA nanocomposites are shown in Fig. 1D. Raman spectrum of the sample was prepared at 500 °C, it reveals entire Raman active mode appeared at the seven (993, 692, 527, 406, 278, 192, 139 cm^{-1}) frequencies vibration mode shown by Fig. 1D. Fig. 1D a, b shows a Raman

spectrum of V_2O_5, V_2O_5/PVA which exhibited the strong powerful peak present at 139 cm^{-1} corresponds to the Bg symmetry and the large in vibration frequency at 990 cm^{-1} corresponding to stretching of O—V—O atoms was observed. The bending and stretching vibration mode appeared at 278, 406 and 527 cm^{-1} areconsequential beginning the bending mode of V—O band and 692 cm^{-1} stretching mode to correspond to the parallel and perpendicular plane. Alsoto Fig. 1D (c, d) is a extremelyacceptable tool to scrutinize the disorders of carbon based material (Hong et al., 2017; Berenguer et al., 2017). Therefore, the V_2O_5 was intrigued by Raman spectra. Fig. 1D (c, d) shows a Raman spectrum of V_2O_5/G-C_3N_4 which exhibited the typical two broad band's at 1345 and 1590 cm^{-1} for the disordered (D) band and graphitic (G) band. The mainly observed the G band was ascribed the sp^2 hybridized carbon atom, which ascribed to the 1st order dispersion of the stretching vibration (E_{2g}). The large intensity peak of G band pronounces hashigh crystallinity compound. On the other hand, the D band corresponds to structural disorders and defects which contravention the sp^2 symmetry carbon. These defects and disorders weregenerallyfashioned by the occurrence of heteroatom, which collapses the controlled crystallization of carbon to the lattice structure of hexagonal shape. These disorder and defects was mostlyfashioned by the incidence of hetero atoms, which collapses the structured crystallization of carbon to the hexagonal lattice (Tadyszak et al., 2018). The intensity ratios (G/D ratio) 0.71 and 1.2 are observed which corresponds to V_2O_5/G-C_3N_4 and V_2O_5/G-C_3N_4/PVA nanocomposite respectively.

The size and morphology of the V_2O_5, V_2O_5/PVA, V_2O_5/G-C_3N_4, V_2O_5/PVA/G-C_3N_4 the nanocomposite are shown in Fig. 2A. FE-SEM image of V_2O_5 (Fig. 2Aa), clearly shows the nanosheet shape. Fig. 2Ab and c are showed the characteristic FE-SEM images of the V_2O_5/PVA (agglomerated image for sheet shape), and V_2O_5/G-C_3N_4 (nanosheet) and it is randomly distributed. But in Fig. 2Ad and f indicated that the formation of agglomerated sponges like nanosheet structure of V_2O_5/PVA/G-C_3N_4 nanocomposite (Takahashi et al., 2004). The V_2O_5/PVA/g-C_3N_4 nanocompositeprovides superiorexterior area, superior surface motion and well-organized transmission direct for discovery of analytes and helped to achieve the active sites, to improve the sensitivity of the nanocomposite surface modified electrode. Fig. 2Aeis showed corresponding to the EDX spectrum of V_2O_5/PVA/G-C_3N_4, which confirms the appearance of the following elements such as V, O, C, and N. The EDX spectrum was obtained by agood qualityconcurrence with the reported nanocomposite investigated by the spectrum of EDX. The elemental coloured mapping images in Fig. 2B (a–d) fairly showed the V (red), O (green), N (yellow) and C (blue) elements in the material without any other significant impurities. The unique morphology of V_2O_5/PVA/G-C_3N_4nanocomposite is confirmed by HR-TEM, as illustrated in Fig. 3. From Fig. 3a we substantiate that the plate of hexagonal shape was occurred linkinghuge size particles of V_2O_5 and nanosheets of G-C_3N_4 to appearancePVA surface. Compared with PVA, the image of V_2O_5/G-C_3N_4 displays the hexagonal like structure and an increased thickness is attributed to the covalently grafting of PVA on the exterior of G-C_3N_4 sheets. The TEM micrograph of V_2O_5/PVA exposes the formation of rectangular like shape as well as the homogeneous distribution of G-C_3N_4) nanoparticles with an average size of ~5–15 nm. Fig. 3b indicates that the crystalline nature of V_2O_5/PVA/G-C_3N_4nanocomposite is observed in the selected area of the electron diffraction (SAED) (Ishii et al., 2017; Kong et al., 2017).

3.2. Electrochemical impedance spectroscopic (EIS) analysis

The electrochemical impedance spectroscopy (EIS) is an important tool to study the electron transfer properties of the nanocomposite modified GC electrodes. The EIS parameters are evaluated using Randles circuit model. Electrochemical impedance spectroscopy (EIS) is studied from 100 kHz to 0.1 Hz in ferro/ferric couple solution with 0.1 M KCl as a supporting electrolyte. All the EIS spectra shows a depressed semicircle, which attributes to the electro transfer/charge transfer resistance process (Rct) and a linear Warburg part attributes to the diffusion controlled process in the modified GC electrode. The EIS spectra of a) bare GCE, b) V_2O_5/GCE, c) V_2O_5/PVA/GCE, d) V_2O_5/G-C_3N_4/GCE, and e) V_2O_5/PVA/G-C_3N_4/GCE are shown in Fig. 4. All the EIS spectrum of modified and unmodified GCE shows depressed semicircles of different parameters, which is due to different Rct values of the electrodes. The EIS parameters are evaluated from view software using Nyquist plot (Rct) of e) V_2O_5/PVA/G-C_3N_4/GCE was measured 45.18. On the other hand, the Rct value of (a) bare GCE, (b) V_2O_5/GCE, c) V_2O_5/PVA/GCE and d) V_2O_5/G-C_3N_4/GCE were measured to be 235.57, 101.4, 82.1 Ω and respectively, V_2O_5/PVA/G-C_3N_4/GCE is apparently flavorable for fast electron transfer at the interface between the modified electrode and supporting electrolyte.

3.3. Electrochemical behavior of FA in V_2O_5/PVA/G-C_3N_4/GCE

The electrochemical performance of FA was carefully investigated at the bare GCE, V_2O_5, V_2O_5/PVA, V_2O_5/G-C_3N_4 and V_2O_5/PVA/G-C_3N_4 modified GCE. Fig. 5 shows the CV response of bare GCE (curve a), V_2O_5 (curve b), V_2O_5/PVA (curve c), V_2O_5/G-C_3N_4 (curve d) and V_2O_5/PVA/G-C_3N_4 (curve e) modified GCE in the presence of 50 μM FA containing 0.1 M PBS at a scan rate of 50 mV/s. As shown in Fig. 5 (curve a), here is no oxidationFA peak was observed, in the part of unmodified GCE, which suggestedto the oxidation FA peak is not detected individually at the bare GCE. Compared with bare GCE, oxidation peak with rather weaker peak currents are presented at V_2O_5, V_2O_5/PVA, and V_2O_5/G-C_3N_4 modified GCEs, indicating the oxidation peak of FA can be separated with the low electrochemical response as shown in Fig. 5 (curve b–d). In contrast, the V_2O_5/PVA/G-C_3N_4 modified electrode (Fig. 5 (curve e)), well-defined oxidation peak with the peak separation up to 50 mV is exhibited indicating that the irreversible oxidation reaction of catechol to 1, 2-benzoquinone is achieved (Ishii et al., 2017). This increase is largely attributed to the higher surface area of the flake-like shape V_2O_5 decorated on to the surface of covalently grafted G-C_3N_4 with PVA which enhances the electron transfer rate. Also, the ternary nanocomposite exhibits strong synergistic effect which arises due to the inter-constituent interactions between V_2O_5, G-C_3N_4, and PVA resulting in the improvement of the high electron transfer with enhanced electrochemical performance (Nie et al., 2013; Li et al., 2019). The oxidation potential of FA at the modified V_2O_5/PVA/

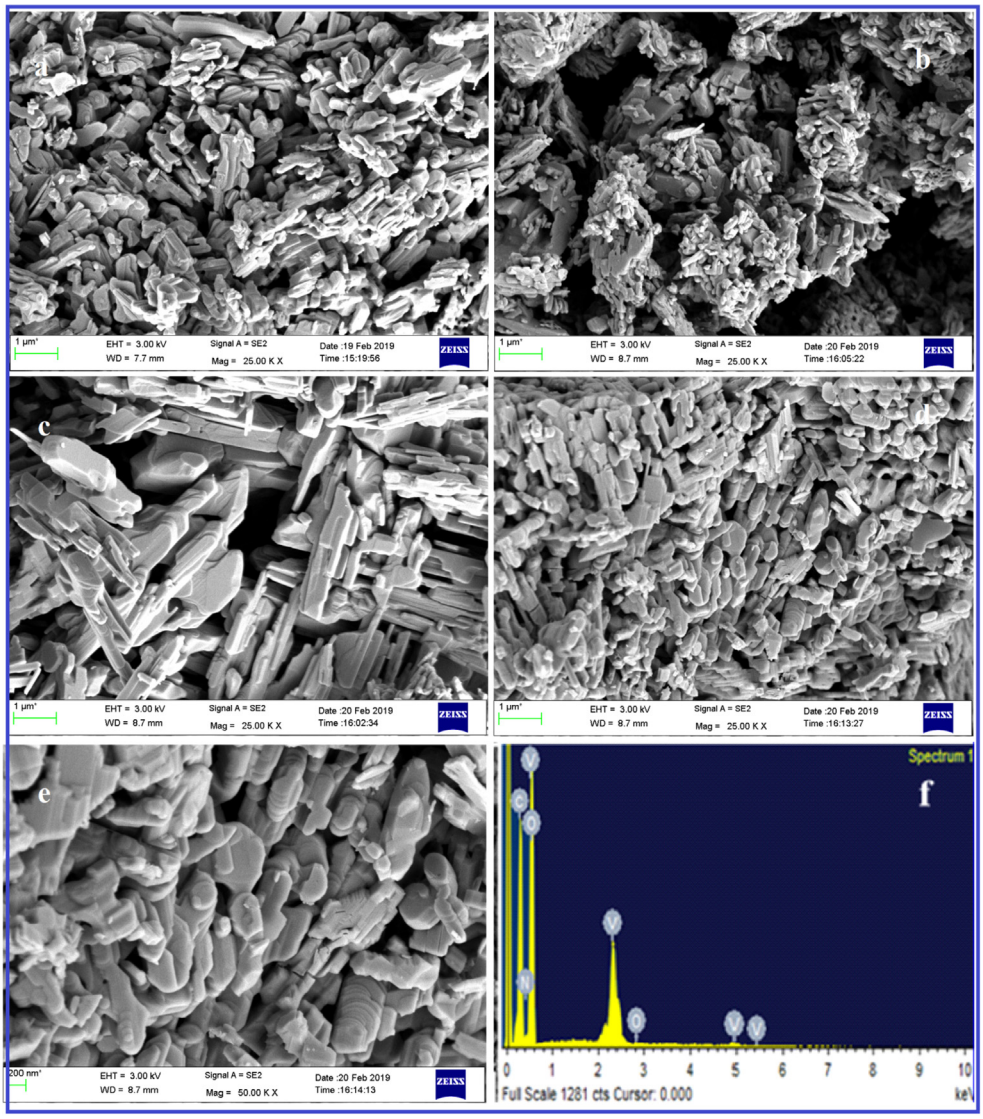

A

Fig. 2 **(A)** FE-SEM high magnification image of (a) V_2O_5, (b) V_2O_5/PVA, (c) V_2O_5/G-C_3N_4, (d & e) different magnification of V_2O_5/PVA/G-C_3N_4 nanocomposite and (f) EDAX spectrum of V_2O_5/PVA/G-C_3N_4 nanocomposite, (B) mapping analysis of V_2O_5/PVA/G-C_3N_4 nanocomposite.

G-C_3N_4 modified electrode (Epa = 0.69 V) is obtained. The increment of peak current of L-tyrosine depends on mass transport properties between electrolyte and electrode involves in this present study Liu et al., 2019b. Hence, the V_2O_5/PVA/G-C_3N_4 modified electrode shows a better performance toward the sensing of L-tyrosine. Furthermore, the electroactive surface area of V_2O_5/PVA/G-C_3N_4 modified electrode was evaluated by using the Randles-Sevcik equation as follows

$$ip = 2.69\ 10^5 n^{3/2} A D^{1/2} C \upsilon^{1/2}$$

where D is the diffusion coefficient of $[Fe(CN)_6]^{3/4}$ ($cm^2\ s^{-1}$), ip is the anodic peak current (A), C is the concentration of $[Fe(CN)_6]^{3/4}$ (mol cm^{-3}), A is the electroactive area (cm^2), n is the number of transferred electrons, and $m^{1/2}$ is the square root of scan rate (V^{s-1}). The estimated active surface area values are 0.5 and 0.69 cm^2 for (a) bare GCE, (b) V_2O_5/GCE, (c) V_2O_5/PVA/GCE, d) V_2O_5/G-C_3N_4 modified electrode, respectively. Fig. 6Aa, displays the CV response of V_2O_5/PVA/G-C_3N_4/GCE towards the electrochemical oxidation of FA by different concentration of 10 µM to 120 µM in 0.1MPBS (pH-7) at a constant scan rate of $20Vs^{-1}$. The results proved, there is a linear increase in oxidation current peaks upon the consistent addition of FA. Lastly, the concentration of FA linear plot versus peak current was exhibited and plotted in Fig. 6Ab. The consequent linear regression equation is said to be ipc (µA) = 0.0415x + 0.56, R^2 = 0.9994.

3.4. Influence of scan rate

The transport characteristics of the V_2O_5/PVA/G-C_3N_4 modified GCE was investigated by CVs techniques with various scan rates in 0.1 M PB (pH = 7.0) containing 50 µM of FA

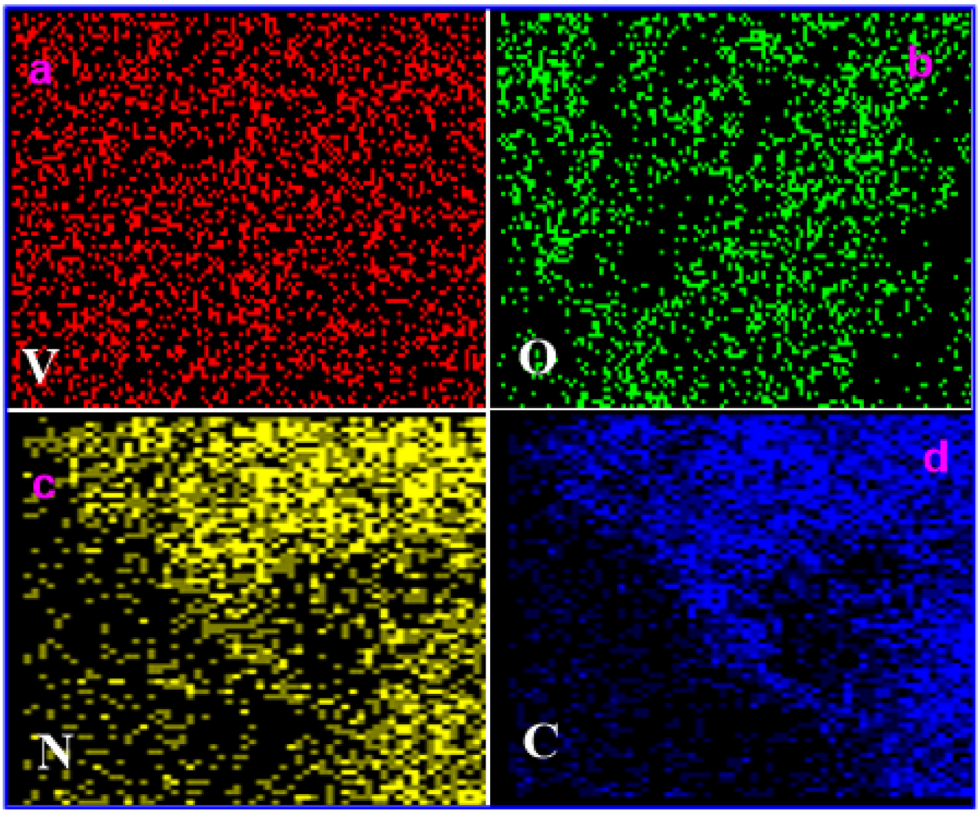

B

Fig. 2 (*continued*)

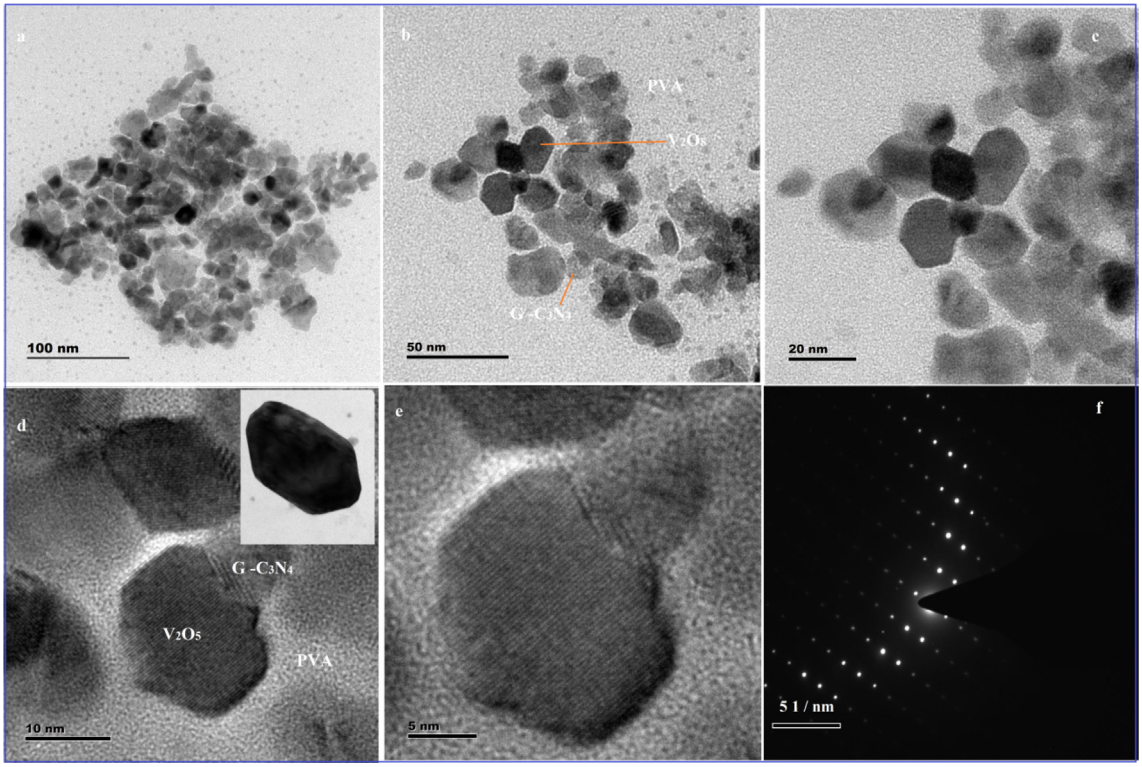

Fig. 3 High magnification TEM image of (a–e) V_2O_5/PVA/G-C_3N_4 nanocomposite and (f) SAED pattern of V_2O_5/PVA/G-C_3N_4 nanocomposite.

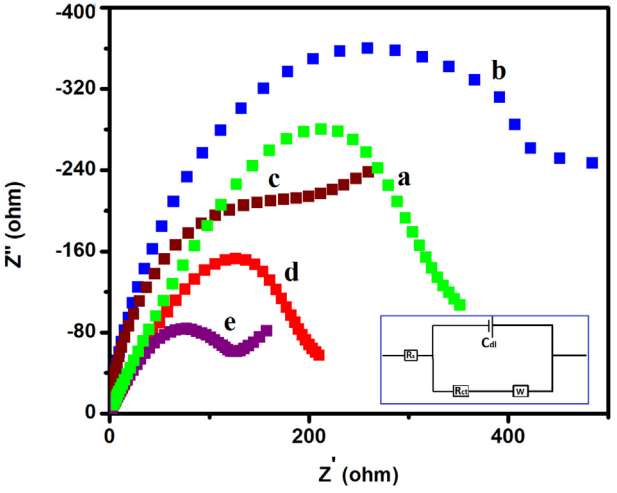

Fig. 4 Electron impedance spectroscopy of (a) bare GCE, (b) V_2O_5/GCE, (c) V_2O_5/PVA/GCE, (d) V_2O_5/G-C_3N_4/GCE, and (e) V_2O_5/PVA/G-C_3N_4/GCE in 0.1 M KCl solution containing $[Fe(CN)_6]^{-3/-4}$.

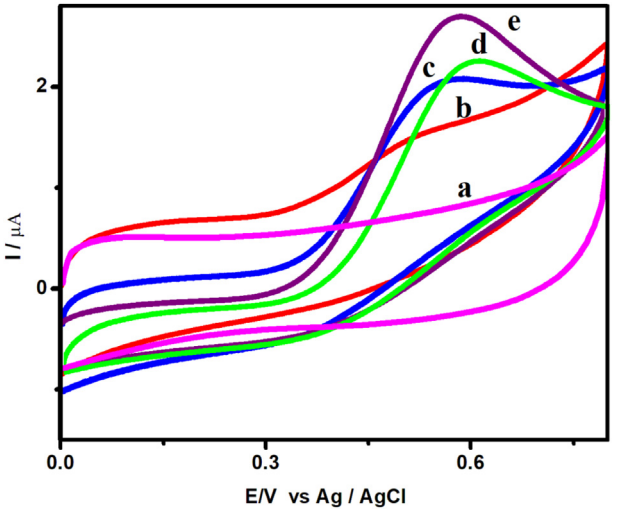

Fig. 5 Cyclic voltammetric response of (a) bare GCE, (b) V_2O_5/GCE, (c) V_2O_5/PVA/GCE, (d) V_2O_5/G-C_3N_4/GCE, and (e) V_2O_5/PVA/G-C_3N_4/GCE in the presence of 50 µM FA containing 0.1 M (pH = 7) PBS at a scan rate of 50 mV/s.

by CV and the obtained results in displayed in Fig. 6Ba (Narayana et al., 2014). Fig. 6Ba reveals the CVs response of the V_2O_5/PVA/G-C_3N_4 modified GCE containing 50 µM FA (pH = 7) at different scan rates from 10 to 110 mV s^{-1}. The revealed that the peak anodic current regularlyenlarged with growing the scan rate from 10 to 110 mV s^{-1} and peak potential was slightly shifted in a more positive direction. The linear relationship was obtained between different scan rate and anodic-peak current, a linear regression equation of Ipa = 0.0377x + 1.0805 with a correlation co-efficient of R^2 = 0.9976, respectively, and depicted in Fig. 6Bb. These obtained results suggested that the electrochemical oxidation of FAat V_2O_5/PVA/G-C_3N_4 modified GCE is a typically adsorption-controlled process (Mirmoghtadaie et al., 2013a, 2013b).

3.5. Optimization of pH

The effect of pH on the response of FA at V_2O_5/PVA/G-C_3N_4 modified GCE was investigated, and the results are shown in Fig. 7a. When the pH of the solution increases from 3.0 to 9.0 (3, 4, 5.5, 6, 7, 8, 9) the maximum peak current is attained at a pH of 7.0. At acidic condition pH, the synthesized composite is protonated and the amine group in FA is not ionized, which decreases the adsorption capacity of UA, thereby producing a high over-potential. FA is unstable in alkaline solution and can be easily oxidized, thus affecting the detection of target molecules. A further increase in pH leads to a decrease in the current peak (Razaei et al., 2018, Harishaet al., 2015; Mirmoghtadaie et al., 2013a, 2013b). Hence, pH 7.0 PBS was used as agood electrolyte in the consequent experiments. A linear plot between the redox peak potential and pH was obtained (Fig. 7b) and values are close to the theoretical value of +0.59 mV/pH, revealing that the number of electrons and protons taking part in the electrode reaction is equal. Thus, the electrochemical oxidation of FA at the V_2O_5/PVA/G-C_3N_4 modified GCE should be a two-electron and two-proton process Tadyszak et al., 2018. The possible electron transfer mechanism for FA at V_2O_5/PVA/G-C_3N_4 modified GCE is shown in Scheme 2.

3.6. Linear sweep voltammetry (LSV)

Fig. 8displayed the electrochemical sensing of FA was employed as investigated by LSV method. While the concentration FA level was enlarged from the linear ranges 0.01–100 µM and the current density peak was observed at 0.6 V, which enhance linearly illustrated in Fig. 8a. Besides, the FAconcentration was increased linearly with increasing the density 0.01–100 µM and the correlation coefficient is 0.991 as shown in Fig. 8b. These consequencesbe synthesized V_2O_5/PVA/G-C_3N_4 modified GCE be able tospecially used as anable electrode material for selective detection of FA.

3.7. Amperometric method

The amperometric method was modified for the determination of FA using V_2O_5/PVA/G-C_3N_4 modified GCE. Fig. 9 depicts the typical steady current state response of FA for different additions of FA concentration ranging from 0.01 to 60 µM in PBS at afunctional potential +0.58 V. A well-defined sharp response was observed for the step by step additions of FA in constantly stirred with PBS (pH-7) (Shpigun and Andryukhina, 2019; Štěpánková et al., 2017; Sharma and Arya, 2019; Maleh et al., 2014; Ensafi et al., 2017). The steady current state of the Sensor reaches surrounded by 3 s, demonstrating the quick response Sensor behaviour. Also, the current peak was plotted against FA concentration, a superior linear connection was observed and the calibration plot was shown in Fig. 9a, b. The detection and quantification limit of the Sensor system is calculated by the formula as shown below:

$$LOD = 3.3S/b$$

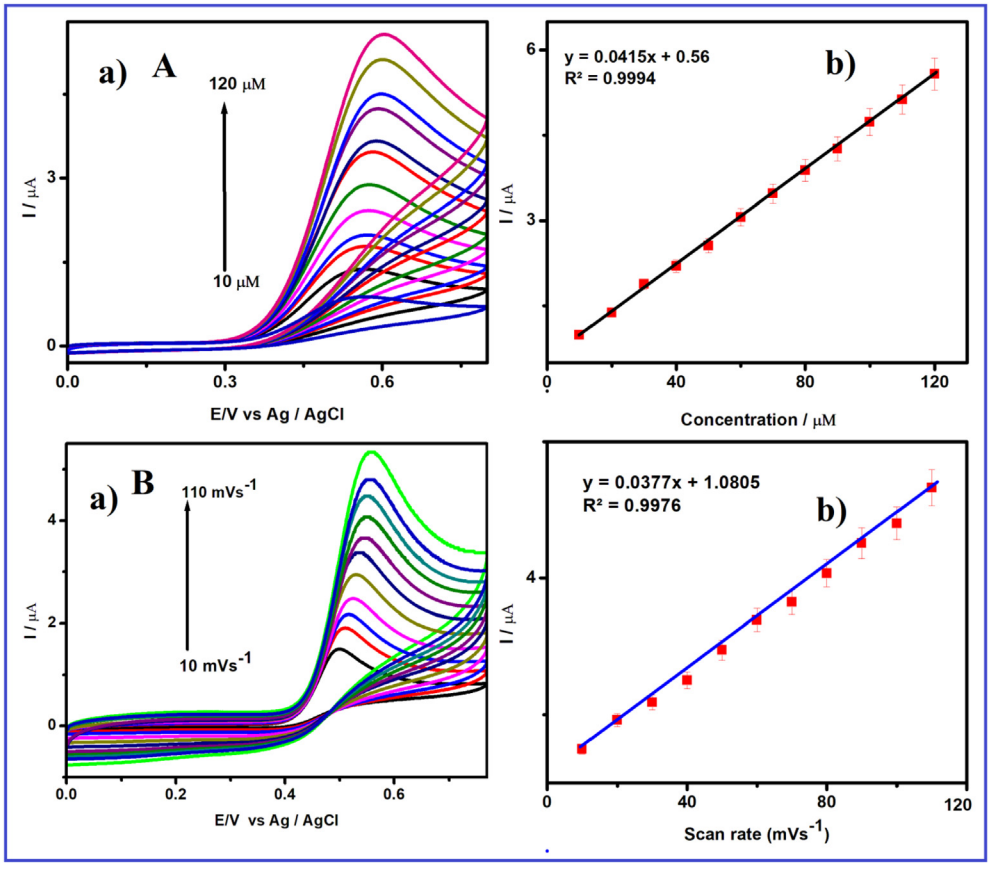

Fig. 6 (A) (a) Cyclic voltammetric response of V_2O_5/PVA/G-C_3N_4/GCE in FA containing 0.1 M (pH = 7) PBS at various concentration from 10 to 120 μM and (b) the linear plot for redox peak current response of FA vs. concentration, (B) (a) Cyclic voltammetric response of V_2O_5/PVA/G-C_3N_4/GCE in 50 μM FA containing 0.1 M (pH = 7) PBS at different scan rates from 10 to 110 mV/s and (b) the linear plot for cathodic peak current response of FA vs. square root of scan rate.

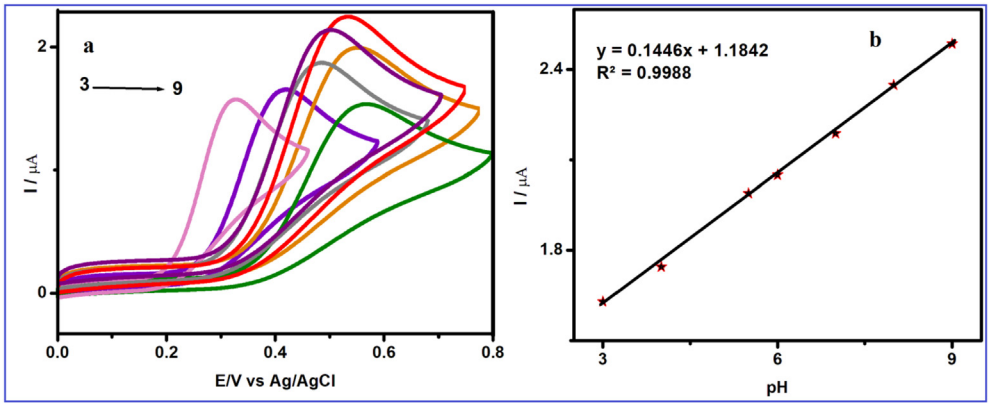

Fig. 7 (a) Cyclic voltammogram obtained at V_2O_5/PVA/G-C_3N_4/GCE in 50 μM FA containing different pH (pH 3, 4, 5.5, 6, 7, 8 and 9) at a scan rate of 50 mV/s (a, c) and (b) Calibration plot for the pH vs. peak potential for the detection of FA.

$$LOQ = 10S/b$$

where S standard deviation of the lowest concentration level of FA, and b calibration curve of the slope obtained from the amperometry (Kalimuthu and John, 2009). The estimated linear range of the Sensor is 0.01–60 μM with a correlation coefficient of 0.9813. The analytical sensitivity of the Sensor is 19.02 μA μM^{-1} cm^{-2} and the limit of detection (LOD) of the Sensor has achieved to be 0.00174 μM witha noise -to- signalratio of 3 (S/N = 3). Based on these abbreviations, the proposed FASensor could improve the analytical parameters especially extensive linear response range and lower LOD than the previously reported FASensor and the consequences are illustrated in Table 1 (Lavanya et al., 2016; Nie et al., 2013; Narayana

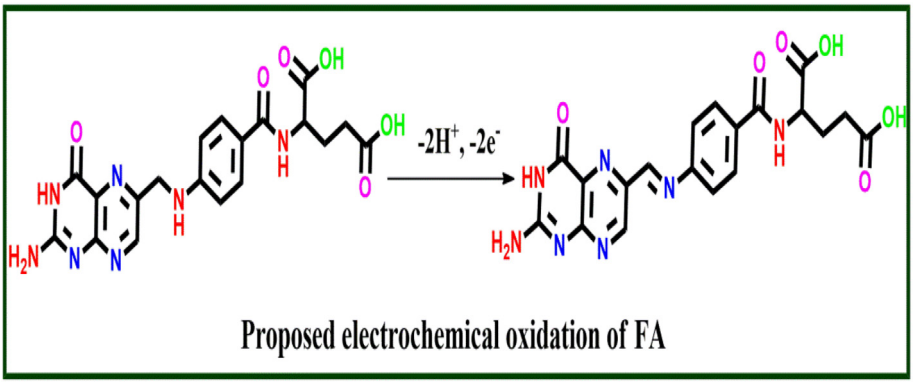

Scheme 2 Proposed mechanism of FA detection.

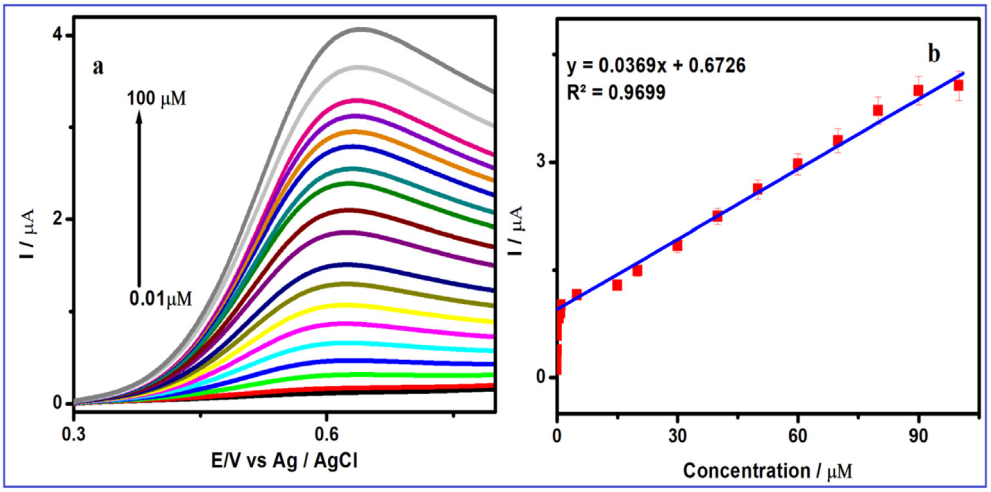

Fig. 8 (a) Linear sweep voltammetric response of V_2O_5/PVA/g-C_3N_4/GCE containing 0.1 M (pH = 7) PBS at various concentration from 1 to 160 µM and (b) the linear plot for redox peak current response of FA vs. concentration.

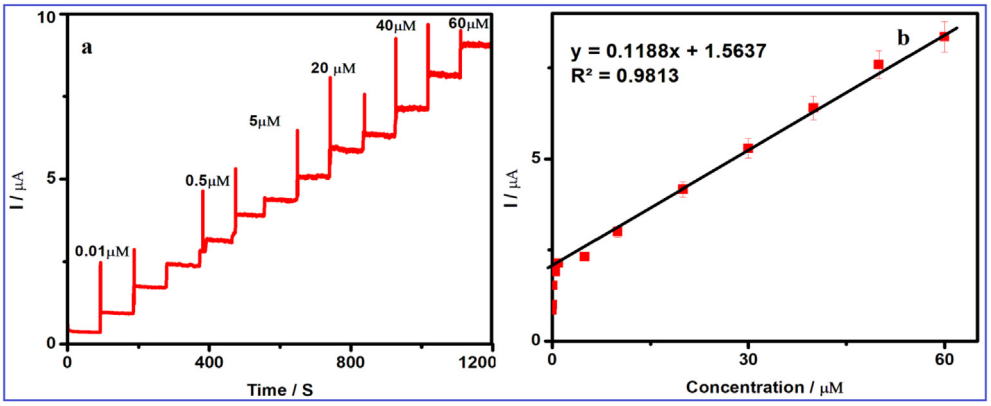

Fig. 9 (a) Amperometric i–t curves for the determination of FA at V_2O_5/PVA/g-C_3N_4/GCE in 0.1 M PBS (pH 7.0). Each addition increases the concentration of 10 µM of FA at a regular interval of 50 s, (b) the calibration plot for the linear dependence of peak current vs. concentrations of FA.

et al., 2014; Mirmoghtadaie et al., 2013a, 2013b; Harisha et al., 2015; Mani et al., 2017). This marvelouspresentation of the Sensor indicates that the outstanding electrocatalytic behaviour of V_2O_5/PVA/G-C_3N_4 modified GCE.

3.8. Selectivity towards FA

The selectivity towards FA at V_2O_5/PVA/G-C_3N_4 modified GCE was explored by the amperometric technique in 0.1 M

Table 1 Detailed comparison of the FA using various electrode materials.

Sensing materials	pH	Method	Linear range (μM)	LOD (μM)	Ref
Poly (Alanine)/CPE	ABS (pH = 5)	CV	10–40	3.40	Harisha et al. (2015)
Graphene/Molybdenum Disulfide Nanosheets/Gold	PBS (pH = 7.4)	Amperometric	50–1150	0.038	Mani et al. (2017)
Au nanoparticles	PBS (pH = 7)	DPV	0.01–1	7.5	Mirmoghtadaie et al. (2013a, 2013b)
Ferrocenedicarboxylic acid/MWCNTs	Universal buffer	DPV	4.6–152	1100	Narayana et al. (2014)
poly(3,4-ethylenedioxythiophene) /SWCNT	PBS (pH = 7)	DPV	0.1–500	0.07	Nie et al. (2013)
Mn-SnO_2/GCE	PBS (pH = 6)	SWV	0.5–900	0.079	Lavanya et al. (2016)
V_2O_5/G-C_3N_4/PVA/GCE	PBS (pH = 7)	Amperometric	0.01–60	0.0017	**This work**

PBS (pH = 7). To evaluate the selectivity of 50 μM FA at V_2O_5/PVA/G-C_3N_4 modified GCE of interfering substances (200 μM) such as (b), L-Valine, (c) L-serine, (d) L-leucine, (e) L-threonine, (f) L- methionine, (g) L-histidine, (h) L-arginine, (i) Ascorbic acid and (j) Dopamine were added in presence of 10 μM of FA as shown in Fig. 9a. Consequently, the intrusive components showed the insignificant current response and it plannedsuitable selectivity to the FA sensing. Fig. 10Aa clearly shows that 100 fold excess of (b), L-Valine, (c) L-serine, (d) L-leucine, (e) L-threonine, (f) L- methionine, (g) L-histidine, (h) L-arginine, (i) Ascorbic acid and (j) Dopamine do not influence the response of steady-state current. Thus, V_2O_5/PVA/G-C_3N_4 modified GCE exhibits a higher selectivity and sensitivity toward the detection of FA.

3.9. Repeatability and durability studies

Repeatability and durability are some of the important criteria in electrochemical sensing for FA detection. To determine the storage stability of the V_2O_5/G-C_3N_4/PVA/GCE, its FA detection performance was monitored every day. During a month storage period, the fabricated modified electrode retained 93.54% of preliminary response current which illuminating-good quality storage strength. Repeatability and reproducibility plannedSensor were evaluated in 0.05 M PBS for fifteen (Fig. 10Ab) repeated measurements containing 50 μM FA. The Sensor exhibits considerable repeatability through relative standard deviation (R.S.D) of 3.82% for five repetitivecapacities which were investigated using single V_2O_5/G-C_3N_4/PVA/GCE (Liu et al., 2019a, 2019b; Luo et al., 2019; Zheng et al., 2018; Xiao et al., 2017). Also, the Sensor exhibits appreciable reproducibility with R.S.D of 3.83% for five independent measurements carried out at 5 different V_2O_5/G-C_3N_4/PVA/GCE.

3.10. Real sample analysis

To investigate the instantaneous monitoring of the Sensor towards the detection of FA in natural samples like broccoli, human urine, human blood serum, oranges, tomato juice, beetroot, papaya juice and commercial folate tablet, the real sample analysis (preparationis presented elaborately as supplementary information (SI) using a standard addition

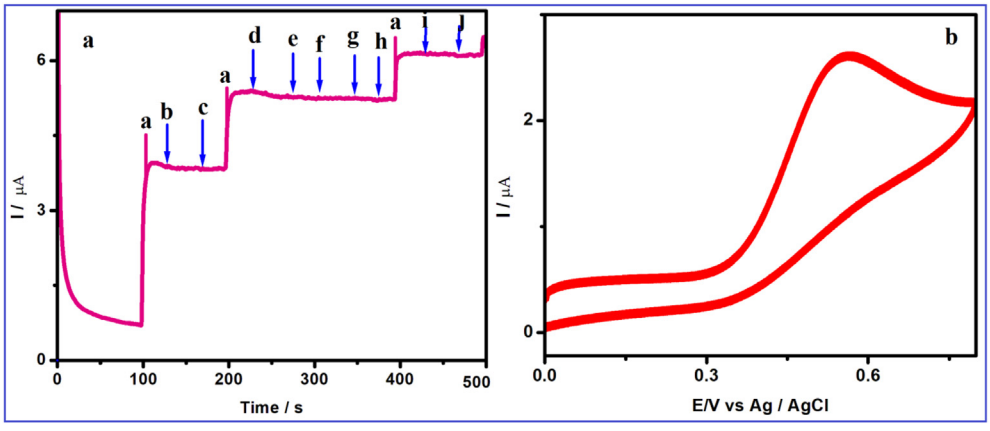

Fig. 10 (A) Amperometric response for V_2O_5/PVA/G-C_3N_4/GCE to successive addition of 10 μM (a) FA in the presence of 200-fold excess of concentrations of (b), L-Valine, (c) L-serine, (d) L-leucine, (e) L-threonine, (f) L- methionine, (g) L-histidine, (h) L-arginine, (i) Ascorpic acid and (j) Dopamine with homogenous stirred with 0.1 M PBS (pH 7.0). (B) Cyclic voltammetric response of V_2O_5/PVA/G-C_3N_4/GCE (30 cycles) confirming the stability of the sensor system in 50 μM L-tyrosine containing 0.1 M (pH = 7) PBS.

Table 2 Determinations of FA in different water samples using the proposed V_2O_5/G-C_3N_4/PVA/GCE.

Real sample analysis	Added (μM)	Found (μM)	Recovery (%)	RSD (%)
Folate tablet	10	9.84	98.4	3.4
	20	19.97	99.9	3.13
Human serum	10	10.12	101.2	3.1
	20	19.85	99.25	3.2
Human urine	10	9.9	99.00	3.7
	20	19.6	98.0	4.1
Oranges	10	9.92	99.2	2.9
	20	19.87	99.35	2.8
Tomato juice	10	9.97	99.7	3.0
	20	19.96	99.8	2.8
Beetroot	10	8.9	89.00	2.7
	20	19.68	98.4	2.9
Papaya juice	10	9.5	95.00	2.5
	20	19.57	97.85	2.9
broccoli	10	9.9	99.00	3.0
	20	19.68	98.4	3.2

method was employed. All these samples are spiked with a known amount of FA and their recovery percent was calculated and are tabulated in Table 2 (Zayed et al., 2018). The planned sensing proposal can be effectivelypractical to the determination of FA in real samples with reasonable recoveries.

4. Conclusion

A novel and efficient V_2O_5/G-C_3N_4/PVA nanocomposite was successfully prepared by an in-situ oxidative polymerization method, and the product was characterized in detail. The electrocatalytic performances of the V_2O_5/PVA/G-C_3N_4 nanocomposite were scrutinized toward the detection of FA. Interestingly, the V_2O_5/PVA/G-C_3N_4 nanocomposite exhibited an electrocatalytic activity as effective and admirable electron mediator for the FA detection. In addition, the V_2O_5/PVA/G-C_3N_4 nanocomposite modified GCE showed low level detection limit, superior sensitivity, wide response linear range, and good quality selectivity smooth in the survival of co-interfering potentially compounds. Besides, V_2O_5/PVA/G-C_3N_4 nanocomposite attained acceptable recoveries to determine FA in broccoli, human urine, human blood serum, oranges, Tomato juice, Beetroot, papaya juice and commercial folate tablet samples. For that admirable electrocatalytic activity of V_2O_5 decorated on G-C_3N_4 covalently grafted to PVA surface, it could be applied for the fabrication of electrochemical Sensor of FA future applications.

Declaration of Competing Interest

The authors have declared no conflict of interest

Acknowledgment

The authors thank the UGC Networking Resource Centre, School of Chemistry, University of Hyderabad, Telangana, India, and the Management of Thiagarajar College for providing necessary facilities to carry out this work.

Appendix A. Supplementary material

Supplementary data to this article can be found online at https://doi.org/10.1016/j.arabjc.2019.12.009.

References

Amanulla, Baishnisha, Sannasi, Sivabharathi, Abubakker, Abdul Kadir Mohamed, Ramaraj, Sayee Kannan, 2018. A magnetically recoverable bimetallic Au-FeNPs decorated on g-C 3 N 4 for efficient photocatalytic degradation of organic contaminants. J. Mol. Liquids 249, 754–763. https://doi.org/10.1016/j.molliq.2017.11.103.

Araú jo, M.M., Marchioni, E., Zhao, M., Kuntz, F., Di Pascoli, T., Villavicencio, A.L.C.H., Bergaentzle, M., 2011. LC/MS/MS identification of some folic acid degradation products after E-beam irradiation. Radiat. Phys. Chem.doi: http://doi.org/10.1016/j.radphyschem.2011.11.029

Berenguer, R., Guerrero-Pérez, M.O., Guzmán, I., Mirasol, J.R., Cordero, T., 2017. Synthesis of vanadium oxide nanofibers with variable crystallinity and V^{5+}/V^{4+} ratios. ACS Omega 2, 7739–7745.

Chen, X., Zhou, Q., Zhang, T., Wang, C.X., Yu, Z., Ahamada, H., Bai, Z., Huang, X., 2019. Development of a sensitive chemiluminescence immunoassay for the quantification of folic acid in human serum. J. Anal. Mathods Chem. 7, 5402903.

Darkwah, W.K., Oswald, A., 2019. Photocatalytic Applications of Heterostructure Graphitic Carbon Nitride: Pollutant Degradation, Hydrogen Gas Production (water splitting), and CO_2 Reduction. Nanoscale Res. Lett. 234, 1063.

Dou, T., Zang, L., Zhang, Y., Sun, Z., Sun, L., Wang, C., 2019. Hybrid g-C_3N_4 nanosheet/carbon paper membranes for the photocatalytic degradation of methylene blue. Mater. Lett. 244, 151–154.

Ensafi, A.A., Esfahani, P.N., Rezaei, B., 2017. Simultaneous detection of folic acid and methotrexate by an optical Sensor based on molecularly imprinted polymers on dual-color CdTe quantum dots. Anal. Chim. Acta 996, 64–73.

Ensafi, A.A., Maleh, H.K., 2010. Modified multiwall carbon nanotubes paste electrode as a Sensor for simultaneous determination of 6-thioguanine and folic acid using ferrocenedicarboxylic acid as a mediator. J. Electroanal. Chem. 640, 75–83.

Fayemi, O.E., Adekunle, A.S., Kumara Swamy, B.E., Ebenso, E.E., 2018. Electrochemical Sensor for the detection of dopamine in real samples using polyaniline/NiO, ZnO, and Fe_3O_4 nanocomposites on glassy carbon electrode. J. Electroanal. Chem. 818, 236–249.

Harisha, K.V., Kumara Swamy, B.E., Jayadevappa H., Vishwanath, C.C., 2015.Voltammetric Determination of Folic acid in presence of Dopamine and Ascorbic Acid at Poly (Alanine) Modified Carbon Paste Electrode. Anal. Bioanal. Electrochem. 7, 454–465.

He, Y., Wang, S., Wang, J., 2016. Detection and quantification of folic acid inserum via a dual emission fluorescence nanoprobe. Anal Bioanal. Chem. 1, 1–7.

Hong, Y., Yang, J., Fan, H., 2017. Controllable synthesis of various V_2O_5 micro-/ nanostructures as high performance cathodes for lithium ion batteries. Cryst. Eng. Comm. 19, 716–721.

Ishii, K., Kimura, Y., Yamazaki, T., Oaki, Y., Imai, H., 2017. Evalation analysis of $V_2O_5.nH_2O$ gels for preparation of xerogels having a high specific surface area and their replicas. RSc. Adv. 7, 35711–35716.

Kalimuthu, P., John, S.A., 2009. Selective electrochemical Sensor for folic acid at physiological pH using ultrathin electropolymerised film of functionalized thiadiazole modified glassy carbon electrode. Biosens. Bioelectron. 24, 3537–3580.

Keyvanfard, M., Ensafi, A.A., Karimi-Maleh, H., Alizad, K., 2012. Modified multiwalled carbon nanotubes paste electrode as a Sensor for the electrocatalytic determination of N-acetylcysteine in the presence of high concentrations of folic acid. Anal. Methods 4, 3268–3274.

Lapa, R.A.S., Lima, J.L.F.C., Reis, B.F., Santos, J.L.M., Zagatto, E. A.G.,1997. Photochemical-fluorimetric determination of folic acid in a multicommutated flow system. Anal. Chem. acta.351, 223–228.

Lavanya, N., Fazio, E., Neri, F., Bonavita, A., Leonardi, S.G., Neri, G., Sekar, C., 2016. Electrochemical Sensor for simultaneous determination of ascorbic acid, uric acid and folic acid based on Mn-SnO_2 nanocomposite modified glassy carbon electrode. J. Electroanal Chem. 770, 23–32.

Li, M., Kong, F., Wang, H., Li, G., 2017b. Synthesis of vanadium pentoxide (V_2O_5) ultra long ofnonobelts via an oriented attachmentgrowth mechanism. Crys. Eng. Comm. 13, 5317–5320.

Li, H., Wang, J., Liu, X., Sun, Q., Djurisic, A.B., Xie, M., Mie, Y., Tang, C.Y., Shih, K., 2017a. Template- free synthesis of hierarchical hollow V_2O_5 microspheres with highly stable lithium storage capacity. RSC Adv. 7, 2480–2485.

Li, D., Xu, H.Q., Jiao, L., Jiang, H.L., 2019. Metal-organic frameworks for catalysis: State of the art, challenges, and opportunities. EnergyChem. 1, 100001.

Liu, X., Zeng, J., Yang, H., Zhou, K., Pan, D., 2018.V2O5-Based nanomaterials: synthesis and their applications. RSC Adv. 8, 4014–4031.

Liu, S., Jiang, X., Yang, M., 2019b. Electrochemical sensing of L-ascorbic acid by using a glassy carbon electrode modified with a molybdophosphate film. Micro Chim. Acta 186, 445.

Liu, J., Li, F., Liu, W., Li, Xin, 2019a. Effect of calcination temperature on the microstructure of vanadium nitride/nitrogen-doped graphene nanocomposites as anode materials in electrochemical capacitors. Inorg. Chem. Front. 6, 164–171.

Long, B., Balogun, M.S., Luo, L., Luo, Y., Qiu, W., Song, S., Zhang, L., Tong, Y., 2017. Encapsulated vanadium-based hybrids in amorphous N-doped carbon matrix as anode materials for lithium-ion batteries. Small 13, 41.

Luo, Y., Guo, X., Yuan, M., Yan, Y., Chen, C.G., Pang, H., 2019. γ-MnOOH nanowires hydrothermally reduced by leaves for high-efficiency electrocatalysis of the glucose oxidation reaction. ACS Sustainable Chem. Eng. 7, 8972–8978.

Majumdar, D., Mandal, M., Bhattacharya, S. K., 2019.V2O5 and its Carbon-Based Nanocomposites for Super capacitor Applications. Chem. electro chem. 6, 1623–1648.

Maleh, H.K., Javazmi, F.T., Daryanavard, M., Hadadzadeh, H., Ensafi, A.A., Abbasghorbani, M., 2014. Electrocatalytic and simultaneous determination of ascorbic acid, nicotinamide adenine dinucleotide and folic acid at ruthenium(II) complex-ZnO/CNTs nanocomposite modified carbon paste electrode. Electroanal 26, 962–970.

Maleh, H.K., Hatami, M., Moradi, R., Khalilzadeh, M.A., Amiri, S., Sadeghifar, H., 2016. Synergic effect of Pt-Co nanoparticles and a dopamine derivative in a nanostructured electrochemical Sensor for simultaneous determination of N-acetylcysteine, paracetamol and folic acid. Microchim. Acta. 183, 2957–2964.

Mani, V., Govindasamy, M., Chen, S.M., Subramani, B., Sathiyan, A., Merlin, J.P., 2017. Determination of folic acid using graphene/molybdenum disulfide nanosheets/gold nanoparticles ternary composite. Int. J. Electrochem. Sci. 12, 258–267.

Mirmoghtadaie, L., Ensafi, A.A., Kadivar, M., Shahedi, M., Reza Ganjali, M., 2013b. Highly selective, sensitive and fast determination of folic acid in food samples using new electrodeposited gold nanoparticles by differential pulse voltammetry. Int. J. Electrochem. Sci. 8, 3755–4376.

Mirmoghtadaie, L., Ensafi, A.A., Kadivar, M., Norouzi, P., 2013a. Highly selective electrochemical bioSensor for the determination of folic acid based on DNA modified-pencil graphite electrode using response surface methodology. Mater. Sci. Eng. C 33, 1753–1758.

Naqvi, S.T.R., Shirinfar, B., Hussain, D., Majeed, S., Ashiq, M.N., Aslam, Y., Ahmed, N., 2019. Electrochemical sensing of ascorbic acid, hydrogen peroxide and glucose by bimetallic (Fe, Ni)−CNTs composite modified electrode. Electroanal 31, 851–857.

Narayana, P.V., Reddy, T.M., Gopal, P., Naidu, R., 2014. Electrochemical sensing of paracetamol and its simultaneous resolution in the presence of dopamine and folic acid at a multi walled carbon nanotubes/ poly (glycins) composite modified electrode. Anal. Methods 6, 9459–9468.

Nie, T., Lu, L., Bai, L., Xu, J., Zhang, K., Zhang, O., Wen, Y., Wu, L., 2013. Simultaneous determination of folic acid and uric acid under coexistence of l-ascorbic acid using a modified electrode based on poly(3,4-ethylenedioxythiophene) and functionalized single-walled carbon nanotubes composite. Inter. J. Electrochem. Sci. 8, 7016–7029.

Pravakar, O., Siddaiah, T., Ramacharyulu, P.V.R.K., Gopal, N.O., Ramu, Ch., Nagabhushan, H., 2019. Spectroscopic, thermal, structural and electrical studies on VO^{2+} ions doped PVA/MAA: EA polymer blend films. J. Sci. Adv. Mater. Device. 4, 267–275.

Razaei, R., Foroughi, M.M., Beitollahi, H., Beitollahi, R., Alizadeh, R., 2018. Electrochemical sensing of uric acid using a ZnO/graphene nanocomposite modified graphite screen printed electrode. Rus J of. Electrochem. 54, 860–866.

Safaei, M., Beitollahi, H., Shishehbore, M.R., 2018. Simultaneous determination of epinephrine and folic acid using the Fe_3O_4@SiO_2/GR nanocomposite modified graphite. Russian J. Electrochem. 54, 851–859.

Sathiya, M., Prakash, A. S., Ramesha, K., Tarascon, J.M., Shukla, A. K., 2011.V2O5-Anchored Carbon Nanotubes for Enhanced Electrochemical Energy Storage. J. Am. Chem. Soc.13340, 16291–16299.

Sharma, A., Arya, S., 2019. Economical and Efficient Electrochemical Sensing of FA using a Platinum Electrode Modified with Hydrothermally Synthesized Pd and Ag Co-Doped SnO_2 Nanoparticles. J. Electrochem. Soc. 166, B1107–B1115.

Shash, N., 2013. Effect of vanadium pentoxide on the electrical, dielectric, and optical properties of poly(vinyl alcohol)/vanadium pentoxide nanocomposites. Ionics. 19, 12.

Shishehbore, M.R., Sheibani, A., Haghdost, A., 2011. Kinetic spectrophotometric method as a new strategy for the determination of vitamin B_9 in pharmaceutical and biological samples. Spectrochim. Acta Part A 81, 304–307.

Shpigun, L.K., Andryukhina, E.Y., 2019. A New Electrochemical Sensor for Direct Detectionof Purine Antimetabolites and DNA Degradation. J. Anal. Mater. Chem. 15, 72526.

Štěpánková, M., Šelešovska, R., Janíková, L., Chýlková, J., Švancara, I., 2017. Sensitive electrochemical Sensor for the determination of FA based on a bismuth-film electrode. Monatshefte für Chemie – Chemical Monthly 148, 423–433.

Tadyszak, K., Majchrzycki, Ł., Szyller, Ł., Scheibe, B., 2018. Preparation and characterization of partially reduced graphene oxide aerogels doped with transition metal ions. J. Mater. Sci. 53, 16086–16098.

Taherkhani, A., Maleh, H.K., Ensafi, A.A., Beitollahi, H., Hosseini, A., Khalilzadeh, M.A., Bagheri, H., 2012. Simultaneous determination of cysteamine and folic acid in pharmaceutical and biological samples using modified multiwall carbon nanotube paste electrode. Chinese Chem Lett. 23, 237–240.

Takahashi, K., Limmer, S.J., Wang, Y., Cao, G., 2004. Synthesis and electrochemical properties of single-crystal V2O5 nanorod arrays by template-based electrodeposition. J. Phys. Chem. B.108, 9795–9800.

Vora, A., Riga, A., Dollimore, D., 2002. Thermal stability of FA. Thermochim. Acta 392, 209–220.

Xiao, X., Zheng, S., Li, X., Zhang, G., Guo, X., Xue, H., Pang, H., 2017. Facile synthesis of ultrathin Ni-MOF nanobelts for high-efficiency determination of glucose in human serum. J. Mater. Chem. B 5, 5234–5239.

Xu, M., Zhang, X., Gao, S., Cheng, X., Rong, Z., Xu, Y., Zhao, H., Huo, L., 2013. Construction of mono dispersive vanadium pentoxide hollow spheres via a facile route and triethylamine sensing property. Cryst. Eng. Comm. 15, 10123–10131.

Young, J.E., Matyska, M.T., Pesek, J.J., 2011. Liquid chromatography/mass spectrometry compatible approaches for the quantitation of folic acid in fortified juices and cereals using aqueous normal phase conditions. J. Chromatogr. A 1218, 2121–2126.

Zayed, A., Bustami, R., Alabsi, W., El-Elimat, T., 2018. Development and validation of a rapid high-performance liquid chromatography-tandem mass spectrometric method for determination of folic acid in human plasma. Pharmaceuticals (Basel) 11, 52.

Zheng, X.H., Jiang, L.Y., Zhao, L.T., Zhang, Q.Y., Ding, L., 2015. Simultaneous quantitation of folic acid and 5-methyltetrahydrofolic acid in human plasma by HPLC-MS/MS and its application to a pharmacokinetic study. J. Pharm. Anal. 5, 269–275.

Zheng, S., Li, B., Tang, Y., Li, Q., Xue, H., Pang, H., 2018. Ultrathin nanosheet-assembled $[Ni_3(OH)_2(PTA)_2(H_2O)_4]\cdot 2H_2O$ hierarchical flowers for high-performance electrocatalysis of glucose oxidation reaction. Nanoscale 10, 13270–13276.

Zheng, J., Zhang, Y., Guo, M., 2017. Preparation and application of electrochemical barbital Sensor based on molecularly imprinting technique. Wuhan Univ. J. Nat. Sci. 22, 207–214.

Zhu, J., Cao, L., Wu, Y., Gong, Y., Liu, Z., Hoster, H.E., Zhang, Y., Zhang, S., Yang, S., Yan, Q., Ajayan, P.M., Vajtai, R., 2013. Building 3D structures of vanadium pentoxide nanosheets and application as electrodes in supercapacitors. Nano Lett. 13, 5408–5413.